Desalination and Water Treatment
www.deswater.com

doi: 10.5004/dwt.2018.22412

120 (2018) 51–64
July

Influence of modified clay on the structure and performance of polysulfone composite membrane

Shivanand B. Teli[a], Abdelbaki Benamor[a,*], Mustafa S. Nasser[a], Muneer Ba-Abbad[b], Abdul Wahab Mohammad[b]

[a]*Gas Processing Center (GPC), College of Engineering, Qatar University, 2713, Doha, Qatar, email: drshivateli@gmail.com (S.B. Teli), Benamor.abdelbaki@qu.edu.qa (A. Benamor), m.nasser@qu.edu.qa (M.S. Nasser)*
[b]*Department of Chemical and Process Engineering, Faculty of Engineering and Built Environment, University Kebangsaan Malaysia, 43600 Bangi, Selangor, Malaysia, email: muneer711@gmail.com (M. Ba-Abbad), drawm@ukm.edu.my (A.W. Mohammad)*

Received 1 December 2016; Accepted 25 April 2018

ABSTRACT

Highly porous modified clay material with large surface area known as "Filtralite" was used as a filler for the preparation of polysulfone (PSf) composite membranes. Filtralite concentration in the membrane composition was varied from 0, 1, 2 and 3%. The prepared membranes were characterized and their permeation performances were identified using pure water, sodium alginate and humic acid solutions. It was found that the addition of Filtralite to PSf increased the water uptake, hydrophilicity, porosity and surface roughness of the membranes. The obtained results showed that both permeation and antifouling properties of the prepared composite membranes were enhanced with added Filtralite content to the PSf membrane. The experimental results showed that a maximum of 2% Filtralite content can be added for better membrane performances, beyond which the membrane characteristics start to degrade.

Keywords: Polysulfone; Filtralite; Composite membranes; Synthesis; Characterization

1. Introduction

Clay is a term used to describe a group of hydrous aluminum phyllosilicate minerals traditionally classified as hydrated phyllosilicates or hydroxides of silicon, aluminum, magnesium, or other metal ions, either natural or synthetic [1,2]. Clays can also be classified as cationic or anionic based on the charges borne on their constituent layers. Cationic clays contain negatively charged alumino-silicate layers balanced by interlayer cations, and are primarily natural. Anionic clays have positively charged metal hydroxide layers with interlayer regions containing anions, and are mainly synthetic [3]. Tailoring the clay structure on the nanometer scale produces organo-clays with large surface area, and new physical, chemical, and optical properties that are different from bulk solids. A wide range of polymers including organic cations [3,4], poly (dimethylsiloxane) [5], phosphonium [6], poly (ethylene glycol) polymer [7], poly (ethylene oxides) polymer [8], polylactic acid [9], polymethyl methacrylate, and polystyrene [10] have been used as clay montmorillonite modifiers to produce new adsorbents as well as producing new nanocomposites to improve barrier resistance in packaging applications. An example of this, is the production of environmental friendly packaging by improving the mechanical and barrier properties of biodegradable polycaprolactone plastics through dispersed clay nanofillers [11–13]. In general, and depending on the structure and relative position of the clay sheets, there are three ideal structures of polymer/clay composites: (i) the clay sheets can remain bound to one another in separate tactoids; (ii) the polymer can be 'inserted' into the gallery of the interlayer space between the clay sheets to form an intercalated structure; and (iii) the clay sheets can be completely exfoliated to become uniformly distributed throughout the polymer matrix [14]. Intercalation and exfo-

*Corresponding author.

liation of clays can be achieved through adsorption of polymer molecules from a solution into the clay interlayers. In situ polymerization within clay particles is also a common procedure to obtain intercalated/exfoliated polymer/clay composites as shown in Fig. 1.

In the exfoliated clay, the clay sheets are expanded from its normal size of 1 nm to about 20 nm or higher with a relatively uniform dispersion, greatly enhancing various materials properties [15].

To control the state of polymer intercalation within bentonite layers, it is important to understand the thermodynamic conditions, stability of the formulated organo-bentonite dispersion, and kinetic mechanisms of dispersion starting from intercalation of clay layers by the polymer to the full exfoliation of clay sheets. Exfoliation of nanoclay in polymer matrices can provide high-barrier properties and improve thermal and mechanical properties [16]. If the filler used is inert and is compatible with the polymer matrix, it will take up the free volume within the polymer matrix and create tortuous paths for permeating molecules. On the other hand, if the filler is incompatible with the polymer matrix, voids tend to occur at the interface, which tends to increase the free volume of the system, thereby increasing the permeability [17–19]. The continued attention of membrane scientists towards the ability of clays to act as membranes restricting the passage of solutes (e.g., aqueous miscible contaminants) is well documented [20].

Introduction of any kind of clay in the nanoscale level enhances the overall properties of the virgin polymer. Developments in the properties of nanocomposite membranes have been reported in the field of filtration [21,22]. Since membrane technology has an important role in separation techniques for water and wastewater treatment, chemical, metallurgical and petrochemical-related industries and food industries, special attention should be given to the preparation of membranes, especially polymer membranes that are largely used in these separation processes.

Polysulfone (PSf) membranes are polymeric membranes known by their excellent thermal, biological, and chemical stabilities. However, they exhibit low hydrophilicity causing a reduction in water flux and formation of fouling deposits on the membrane surface. Therefore, developing new techniques that could improve these membranes wettability without harming other material properties is of a great importance. The nanocomposite technology is known to be effective in improving the aforesaid properties and improving membranes hydrophilicity. A number of reports on PSf/clay nanocomposite membranes with improved hydrophilicity, mechanical and thermal stability, anti-corrosion, anti-microbial and superior barrier properties are available [23–25]. Clay-incorporated membranes were employed in process separation such as gas separation [26], pervaporation [27], membrane distillation [28], reverse osmosis [28] and ultrafiltration processes [29]. Different researchers tried to alter the hydrophobic PSf membrane surface nature into a hydrophilic one by applying different kinds of clay as fillers. Unmodified (Cloisite Na type) and organically modified (Cloisite 30B and 93 type) clays were used and found to improve the composite membranes hydrophilicity. Amilia et al. [30] incorporated nanoclays in PSf membranes which improved the hydrophilicity, thermal stability and mechanical resistance of the composite membranes. The clays were calcined before application and the synthesized PSf/clay membranes were used for dextran removal from water. The permeation results showed that the synthesized membranes proved to be in the microfiltration range. Mierzwa et al. [31] showed that nanoclay addition increased the membrane contact angle, reduced the negative surface charge density and had no effect on membrane porosity and thickness. Meanwhile, they showed that there was an optimum clay-nanoparticle concentration above which membrane performance was significantly reduced. Ghaemi et al. [32] proved that increasing nanoclay concentrations in membranes results in higher membrane hydrophilicity, porosity and thinner skin layer. Similarly, Ma et al. [22] studied the performance of PSf/clay membranes prepared using non-solvent-induced phase inversion technique and showed that the clay was well dispersed in the PSf matrix and the membrane hydrophilicity was improved.

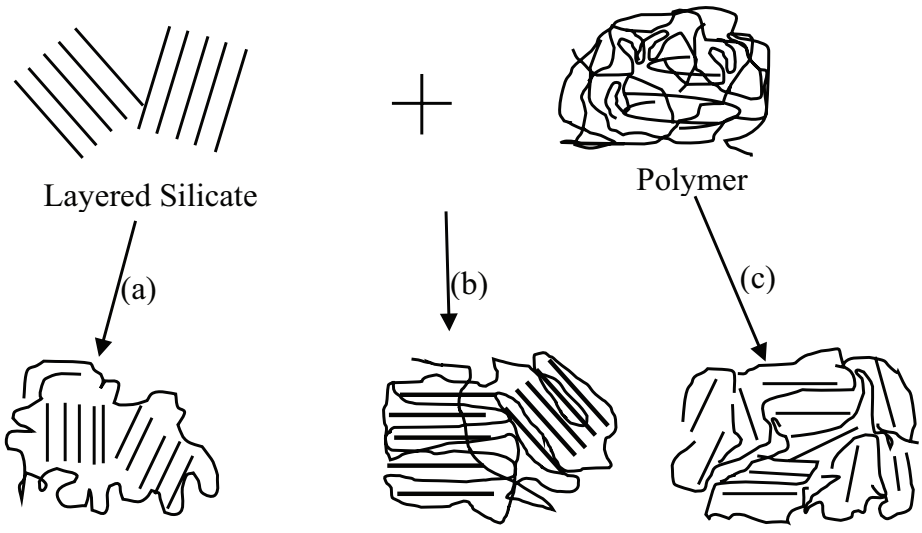

Fig. 1. Three categories of clay-polymer nanocomposites: a) isolated tactoids encapsulated in the polymer matrix; b) intercalated polymers; c) exfoliated clay sheets.

In this work, new PSf-Filtralite composite membranes are fabricated by phase inversion method. Filtralite was selected as the membrane filler because of its ease and availability, cost effectiveness, and hydrophilic nature. The Filtralite high porous structure, large surface area, low density, and aggregate sizes in the range of 0.8–1.6 mm makes it suitable to filtration applications [33]. A high percentage of Si and Al layers in clay impart better dispersion ability to the polymer matrix. The association of these layers with the polymer can produce traditional microcomposites, as well as intercalated and exfoliated nanocomposites, causing a high impact on the membrane performance. To the authors' best knowledge, this is the first study where thermally treated Filtralite clay is incorporated in PSf to produce composite membranes. Produced membranes were employed for the filtration of water, NaAlg and humic acid solutions.

2. Materials and methods

2.1. Materials

Treated clay sample (Filtralite® NC 0.8–1.6) was received from Filtralite Company in Norway (http://www.filtralite.com/en/home-page). The Filtralite sample was a thermally treated normal clay having particle density of 1260 kg/m^3, and bulk, dry, compressed density of 530 kg/cm^3. The clay particle sizes were in the range of 0.8–1.6 mm. Polysulfone pellets (average Mw ~35,000), anhydrous dimethylacetamide (DMAc, purity-99.8%), polyvinyl pyrrolidone (PVP, average Mw ~10,000), bovine serum albumin (BSA, lyophilized powder ≥ 96%), sodium alginate (NaAlg) and Humic acid, (HA, technical grade) were purchased from Aldrich Chemicals, Milwaukee, USA. Deionized (DI) water was used throughout the experiments.

2.2. Membrane preparation

Pristine polysulfone and PSf-Filtralite composite membranes were prepared by phase inversion. The required amount of clay was added into the DMAc solvent and sonicated for 30 min to prevent clay particles agglomeration. 18 wt. % of PSf polymer with 3 wt % of PVP as pore former were added to the solution and stirred continuously for 8 h. The produced homogenous mixture was casted on a polyester fabric support over a glass plate using a 200 µm thickness casting knife. The obtained membrane was immediately immersed in a coagulation bath of deionized water. Once the immersion process was complete, the prepared membrane was cleaned thoroughly with DI water. The clay content in the prepared membranes varied between 1, 2, and 3 wt. %, the resulting membranes were labelled M1, M2 and M3 respectively. Pristine membrane prepared without addition of Filtralite particles was labelled M0.

2.3. Characterization of Filtralite

The morphology of Filtralite was investigated by Scanning electron microscopy (SEM, Philips model XL30E, USA). The elemental composition of the Filtralite was analysed using energy dispersive X-ray **(Model EDS microanalysis system)** analyser. The particle size distribution was characterized by laser scattering and zeta potential analyzer (Zeta sizer Nano ZS (Malvern, UK). D-values method from particle size measurements was used for quantitative comparison. d_{10}, d_{50} and d_{90} were used to signify the midpoint and the range of the particle sizes of used samples. BET Surface area was analyzed using Micromeritics (Chemisorb model 2750, U.K). The crystallinity of the Filtralite was examined using a benchtop Rigaku X-ray mini-II diffractometer (XRD), Japan. The chemical composition of the Filtralite was determined using a Kratos Ultra Axis DLD X-ray Photoelectron Spectroscopy (XPS), UK.

2.4. Characterization of PSf-Filtralite membranes

Mechanical properties of the prepared PSf-Filtralite membranes in term of uniaxial tensile behaviour were characterized using Instron mechanical testing machine (Model- 5566, UK) at room temperature. Specimens with dimensions of 90×10 mm were carefully cut. The thickness of each specimen was measured by a digital caliper. The Young's modulus, maximum tensile stress, yield stress and the elongation at break of the materials were assessed at a crosshead speed of 5 mm/min. the average of five tests for each specimen was taken for each property. Thermo gravimetric (TGA) analysis (PerkinElmer Pyris 1 TGA, USA) of the membrane was performed under nitrogen atmosphere over a temperature range of 30–700°C at a heat rate of 10°C min^{-1}. The surface hydrophilicity of the membrane was examined by measuring the liquid sessile drop contact angle (CA) using Data Physics OCA 20, Germany. The surface and cross-sectional images of the composite membranes were analyzed using scanning electron microscope (SEM, Philips model XL30E, USA). Atomic force microscopy (Model, MFP 3D-Asylum Research, USA) was used to analyze the membranes surface roughness. Membranes pore sizes were determined from the top surface of SEM images using Image J 1.38' software according to the procedure of Barr et al. [34]. Membrane porosity was determined by water uptake method using Eq. (1):

$$\varepsilon = \frac{(M_w - M_d)/\rho}{AL} \tag{1}$$

where M_w is the mass of the wet membrane sample and M_d is the mass of dry membrane sample; A, L, and ρ are the membrane area (cm^2), membrane thickness (cm), and pure water density (g/cm^3) respectively.

2.5. Equilibrium water uptake

Membrane samples were cut into the required size and immersed in DI for 72 h, after which they were taken out of water, their free surface water removed, and weighed instantly. The wet membrane samples were dried for 24 h at 60 ± 3°C and weighted afterward. Using the weights of dry and wet membrane samples, water content percentage was calculated by the following Eq. (2).

$$\%W_c = \frac{(W_w - W_d)}{W_d} \times 100 \tag{2}$$

where W_w and W_d are the weights of wet and dry membranes respectively.

2.6. Membrane filtration

Membranes filtration experiments were carried out using a stainless steel Sterlitech™ CF042P cross-flow apparatus having an effective area of 42 cm² and 18 L tank volume capacity. A schematic diagram of the filtration set up is given in Fig. 2. The membrane permeability was investigated using three different solutions, namely; water, HA, and NaAlg solutions. Before use, HA solution (0.5 g/L) was paper filtered to avoid speedy fouling of the membrane [35]. Filtration experiments were performed under different pressures and constant cross flow velocity of 1.7 LPM and 25°C. The water flux was calculated by Eq. (3)

$$J_w = \left(\frac{V}{A \cdot \Delta t} \right) \tag{3}$$

where V is the volume of permeated solution (L), A is the membrane area (cm²), and Δt is the permeation time (min). Sodium alginate rejection was determined from the measurement of total organic carbon concentration using a Shimadzu device (Model, TOC-L CSH. Japan) following Eq. (4)

$$\%R = \left(1 - \frac{C_p}{C_f} \right) \times 100 \tag{4}$$

where C_p and C_f are NaAlg concentrations in the permeate and feed solutions respectively.

Membrane antifouling study was performed using pure water and sodium alginate. First, pure water flux, J_{w1} (L/m²·h), was measured under 0.2 bar TMP, then, a solution of 0.5 g/L NaAlg was filtered using the same membrane. After that, the membrane was flushed twice with pure water for 10 min each time before pure water flux, J_{w2} (L/m²·h), was measured again through the same membrane. The fouling resistance of the membrane in term of flux recovery ratio (FRR %) was then calculated using Eq. (5)

$$FRR(\%) = \frac{J_{w2}}{J_{w1}} \times 100 \tag{5}$$

3. Results and discussion

3.1. Morphology and elemental analysis of Filtralite

SEM image and elemental analysis of Filtralite are shown in Fig. 3. SEM images showed the presence of irregular particles with monoclinic rectangular blocks structure having dimensions in the range of 0–5 nm. The irregularity of obtained shapes (Fig. 3a) is attributed to defects caused by the synthesis reaction under high temperature conditions. Filtralite chemical analysis is shown in Fig. 3b where significant presence of Si and Al was observed which are the main components of clay minerals. Mg and Fe resulted from isomorphic substitution and Na were present as exchangeable cations. Trace amount of Na was found, confirming that most Na cations were eliminated during clay filtration and washing. Filtralite diffractograms is shown in Fig. 4, the XRD pattern showed five prominent peaks at 21, 26.8, 28, 36.72 and 50.26 2-theta values indicating the polycrystalline nature of Filtralite. The chemical composition of Filtralite surface was studied using XPS analysis results. The elemental composition of Filtralite is summarized in Table 1 which is in good agreement with the literature [36] while its elemental survey spectra is shown in Fig. 5. In addition, BET surface area analysis of Filtralite presented a surface area of 2.266 m²/g. Filtralite particle size distribution showed a positive skew as presented in Fig. 6 with particle sizes ranging from 100 to 2000 nm. The values of d_{10}, d_{50} and d_{90} for the samples are 341, 579 and 852 nm respectively. Furthermore, zeta potential which is an important parameter to understand the state of the nanoparticle surface and predicting the long-term stability of the nanoparticle measured a surface charge of 17.2 mV.

3.2. Membrane characterization

3.2.1. Thermogravimetric (TGA) analysis

Thermo-gravimetric analysis of PSf and PSf-Filtralite composite membranes is shown in Fig. 7. The tests were performed over a temperature range of 50–700°C under

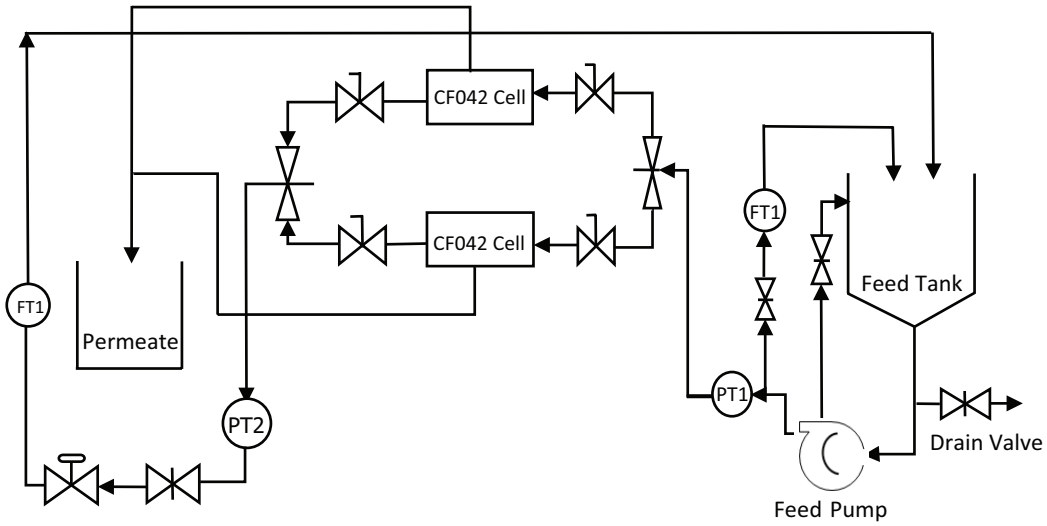

Fig. 2. Schematic diagram of the experimental set-up.

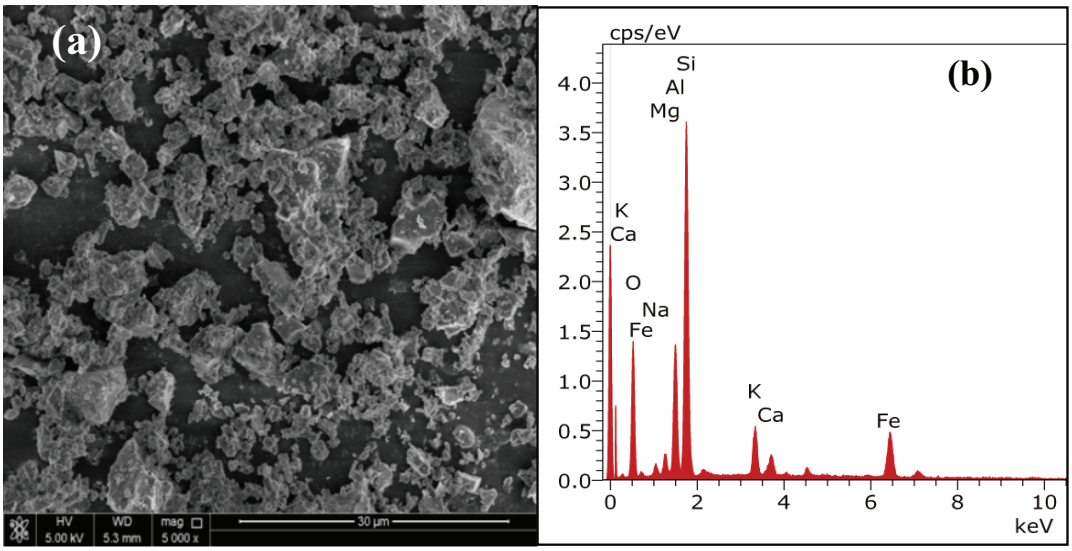

Fig. 3. (a) SEM surface and (b) Elemental results of Filtralite.

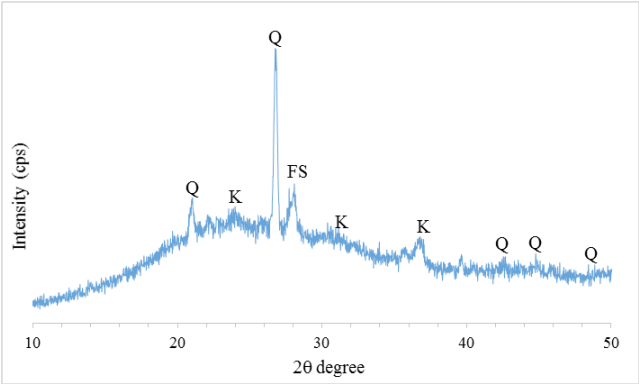

Fig. 4. X-ray diffraction pattern of the Filtralite.

nitrogen atmosphere. The obtained thermogram showed that non-oxidative degradation occurs at three major weight loss regions. The first step, in the 50–160°C region is believed to be caused by water loss. This temperature range progressively shifts to the right with increasing proportion of clay in the membrane (except for M3) due to its enhanced water retention capacity [37]. The second stage, between 450–510°C is attributed to thermal decomposition of PSf [37] while the third step, where higher weight loss was observed is around 510–600°C. These results, revealed that increasing Filtralite concentration the PSf matrix increased the membrane thermal stability. This, may be attributed to the intercalation of polymer matrix into the clay galleries, which act as a fence for thermal degradation of the polymer [25].

3.2.2. Membrane hydrophilicity

Contact angle (CA) results measured for different membranes are presented in Table 2. It is clear that M0 membrane had the highest CA value due to its crystallinity and hydrophobic surface. With the addition of hydrophilic Filtralite in M1 and M2 membranes, the CA values continuously decreases with increasing Filtralite percentage. This could be explained by the hydrophilic nature of Filtralite and the presence of higher percentage of Al and Si elements in the PSf-Filtralite composite membranes, in contrast to M0 in which the vibration of valence bands of Si–O–Si and Si–O–Al are non-existent. The addition of 1 and 2 % of Filtralite in M1 and M2 yielded lower CA values of 60.2° and 51.23° respectively indicating improved membranes hydrophilicity. However, further increase in Filtralite percentage in M3 membrane showed an increase in CA values indicating lower hydrophilicity compared to M1 and M2 membranes. This might be due to Filtralite particle deposition on the membrane surface for Filtralite percentage beyond 2%, which minimizes the formation of homogenous layer on the membrane support.

3.2.3. Membranes morphology

Membranes top surface morphologies for PSf and PSf-Filtralite composite membranes given by SEM images are presented in Fig. 8. Different membranes had different surface pore formation, higher masses of pores were observed on M1 and M2 membranes surfaces, whereas few pores were found on M3 which had higher Filtralite content. The M1 and M2 membranes show interesting pores distribution with modest cracks due to un-melted clay particles structure on the membrane surface. Composite membrane M3 displayed a slight aggregation of Filtralite particles with very few pores on top of the membrane surface compared to M1 and M2. The cross sectional images of the composite membranes shown in Fig. 9, revealed that all membranes possess an asymmetric structure, clearly signifying four distinct layers: a thin dense skin layer at the top surface, supported by a layer of irregular micro-tubular pores, with an open macro-void structure, and porous sponge-like layer at the bottom. The PSf-Filtrate composite membranes presented an interconnected porous structure, without evidence of macro voids in the open pore structure.

Table 1
Elements composition (XPS) and EDX elements data of Filtralite particles

XPS analysis									
Elements	O 1s	C 1s	Na 1s	Al 2p	Si 2p	Fe 2p	Ca 2p	K 2p	Mg
Atomic (%)	53.81	21.65	1.77	5.08	14.41	0.96	1.22	1.11	–
Mass (%)	46.56	14.06	2.20	7.41	21.88	2.89	2.64	2.35	–
Peak BE (eV)	529.0	282.0	1069.0	71.0	99.0	709.0	348.0	290.0	–
EDX analysis									
Atomic (%)	65.42	–	1.74	7.42	18.65	2.48	0.87	1.80	1.63
Mass (%)	49.99	–	1.91	9.57	25.02	6.61	1.67	3.35	1.89

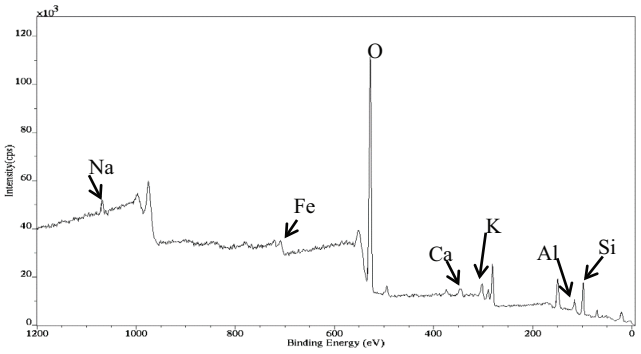

Fig. 5. XPS survey graph of Filtralite particles.

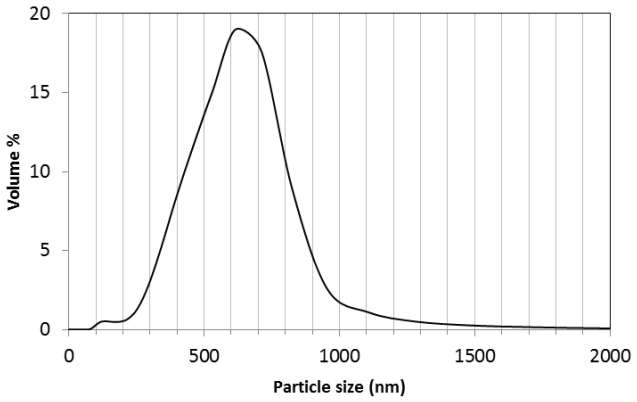

Fig. 6. Average particle size distribution of Filtralite particles in H_2O solution.

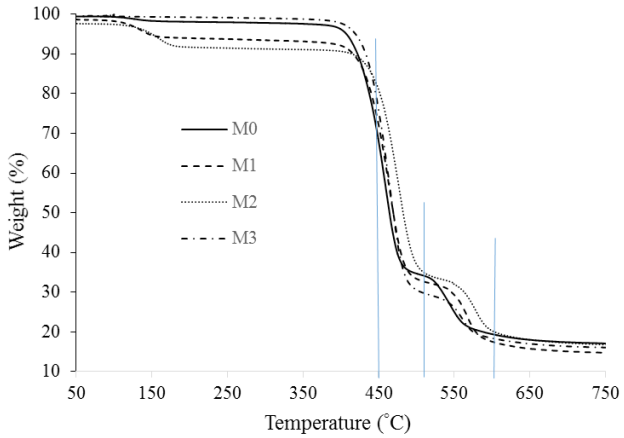

Fig. 7. TGA curves of PSf and PSf-Filtralite composite membranes.

Table 2
Relevant data of water uptake, hydrophilicity and rejection of composite membranes

Membrane	Water uptake (%)	Contact angle (A°)	NaAlg Rejection (%)
M0	46.1 ± 0.6	70.2± 1.8°	86.2 ± 2.1
M1	48.8 ± 1.1	60.2± 2.0°	97.9 ± 1.8
M2	58.0 ±0.9	51.23± 1.5°	98.6 ± 2.3
M3	52.4 ± 0.2	63.78± 1.3°	90.8 ± 1.6

At higher loading of Filtralite, the length of the finger-like projections condensed with increased voids in the sub layer (Fig. 9. M3). The bottom cross section portion of M3 clearly show better dispersion of Filtralite particles in the finger like spongy layer.

3.2.4. Surface roughness

The root mean square (RMS) values of surface roughness of M1, M2 and M3 composite membranes were found to be higher than that of M0 membrane (Table 3). This indicates a larger surface area offered by PSf-Filtralite composite membranes and enhanced membrane permeability. Atomic force microscope (AFM) images presented in Fig. 10 show that dark hydrophilic regions of composite membrane were continuous, forming ion rich channels. Membrane surface with more peaks or valleys represents rougher membrane surface (M0). The addition of Filtralite particles altered the membrane structure thinning the large peaks or valleys of the membranes [31]. However, with higher Filtralite content as in M3 membrane, a higher surface roughness was observed. This might be due to increased viscosity of casting solution that hinders the solvent and non-solvent diffusion during the immersion precipitation process.

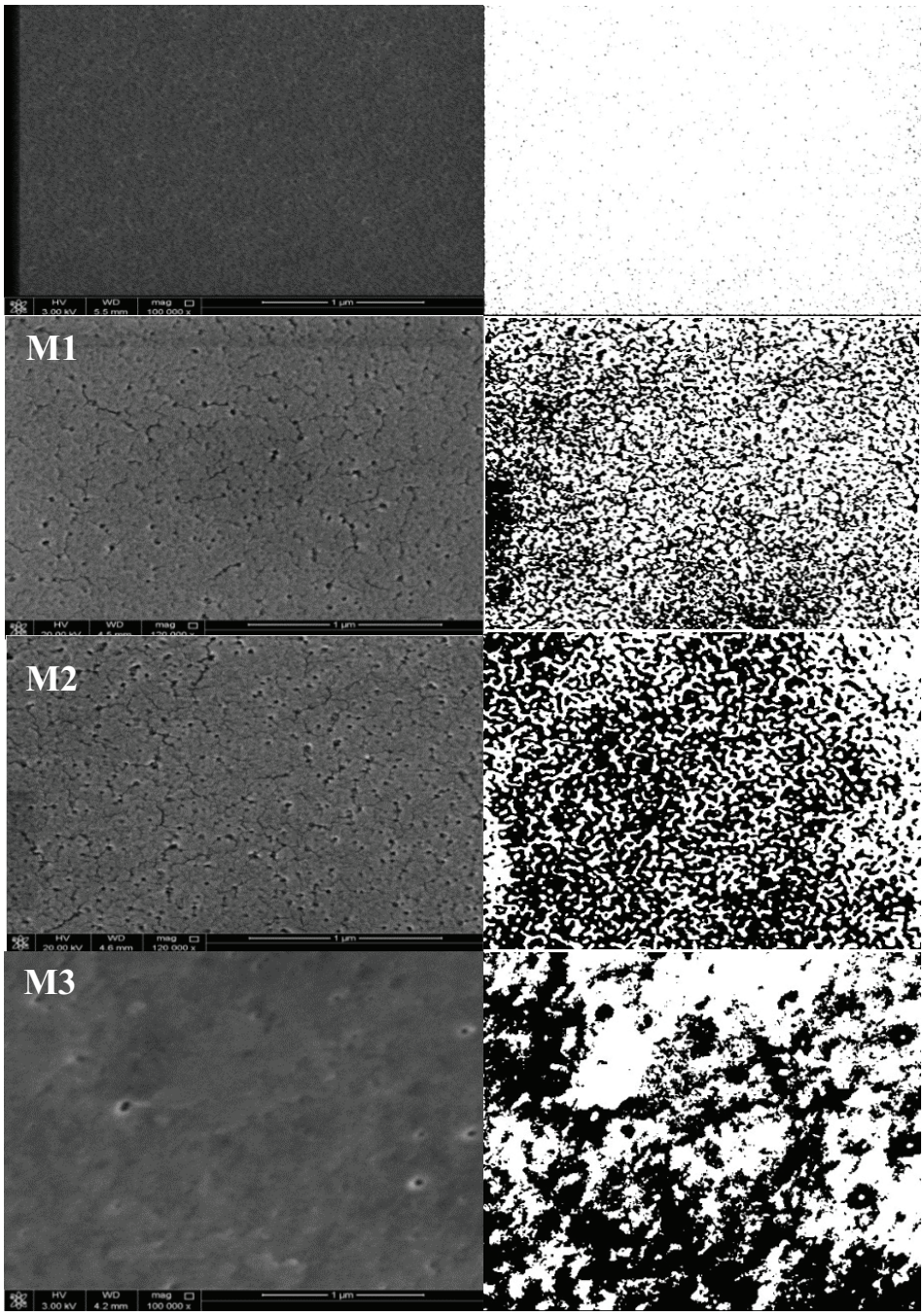

Fig. 8. Top view surface SEM images PSf and PSf-Filtralite membranes.

3.2.5. Water uptake

Water uptake results presented in Table 2 show that all composite membranes (M1, M2 and M3) have higher water uptake compared to M0. Large number of void spaces in the composite membrane allows easy passage of water molecules through surface pores. The Filtralite content with superior hydrophilicity promoted stronger polar interactions with the polymer chains. It was reported that water molecules can be absorbed between clay layers to create an interlayer ionic solution that causes swelling phenomenon related to electrical double layer properties [38,39]. The lower water uptake in M0 resulted from swelling restrictions owing to its crystalline hydrophobic surfaces. On the other hand, the degree of crystallinity of the polymer might decrease in the presence of larger amounts of Filtralite resulting in more free volume for water to diffuse into the membrane matrix as observed in M2. As the amount of Filtralite increases to 3 % (M3), a slight decrease in water uptake was observed. At this stage, some of the clay might be aggregated on the membrane surface restricting the passage of water molecules especially with decreasing membrane crystallinity [40].

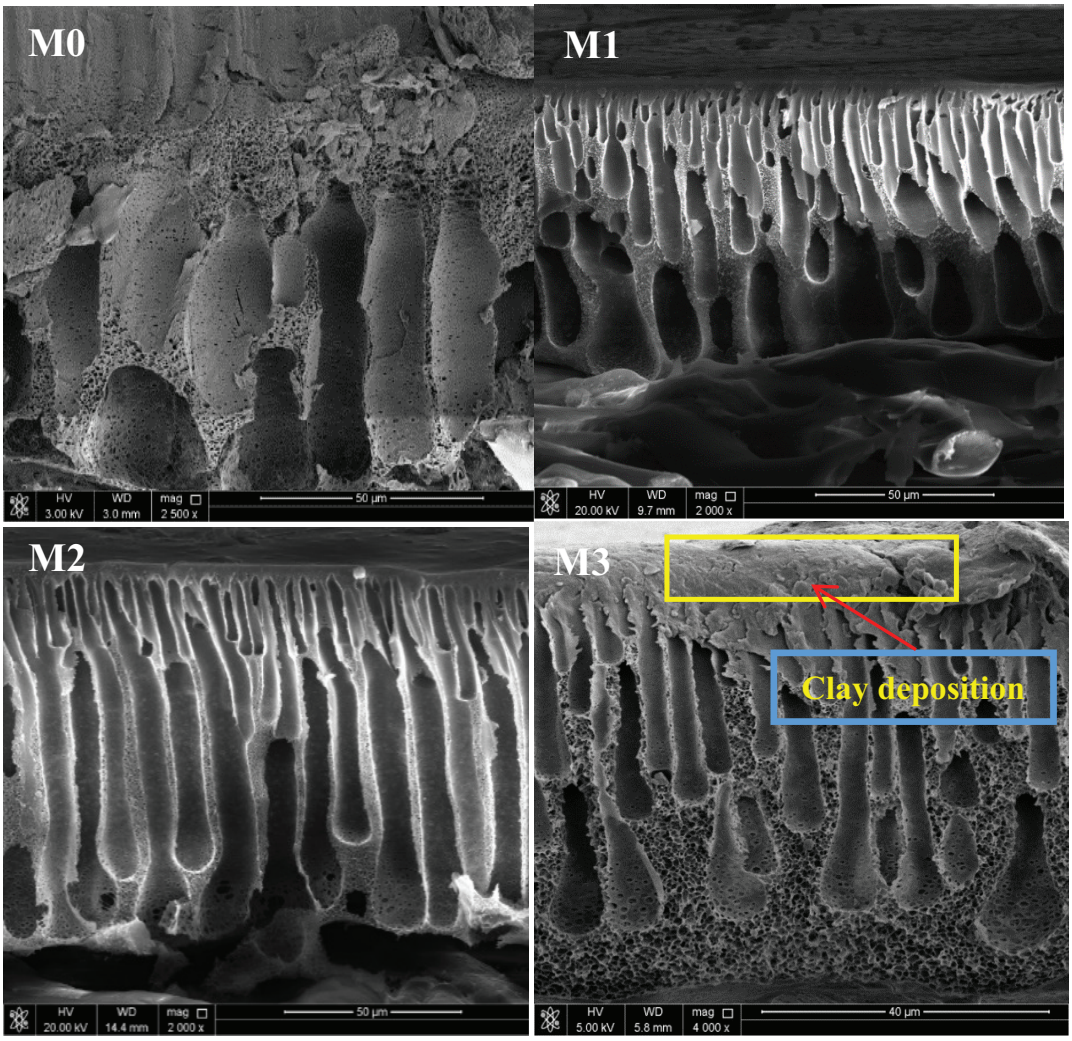

Fig. 9. Cross section SEM images of PSf and PSf-Filtralite membranes.

3.2.6. Surface pore sizes and porosity

The surface pore distributions and surface porosity were determined by analysing SEM images (Fig. 8) using ImageJ software. It was found that addition of 1 and 2% of Filtralite particles and PVP increased the pore diameter and broadened the pore size distribution. These results can justify the improvement in the composite membrane permeability for M1 and M2 [31]. Generally, membrane porosity depends on the mass transfer of the polymer solution during the phase inversion process. The hydrophilic functional groups present in Filtralite would accelerate the membrane formation process by speeding up the exchange rate between solvent and non-solvent. Thus, the pores formation process would be enhanced. The porosity of membranes increased from 51% for M0 to 56% for M2 (Table 3) which are in excellent agreement with those reported in the literature [29]. A slight decrease of porosity in composite membranes M3 was observed. This might be caused by the blockage of the pores and the poor distribution of the Filtralite on the membrane surface due to its agglomeration as supported by SEM images for M3 (Fig. 8). These results are in agreement with the finding of Hussein et al. [41,42]. Furthermore, M3 composite membrane displayed a thick surface with lower porosity which can be attributed to increased viscosity of the casting solution, which resulted in lower water flux in the membrane. The higher average pore size obtained for M2 which is almost twice that of M0, correlates well with the obtained membranes water fluxes. It should be also noted that despite its smaller pore size, M2 membrane had larger water flux M0 due to its higher porosity and improved surface hydrophilicity.

3.2.7. Membranes mechanical properties

Mechnical properties of synthesised membranes are shown in Fig. 11 presenting their nominal stress-strain curves. We observe that the tensile stress increased with increased Filtralite filler amount (M1, M2, and M3). The nonwoven support had the highest Young's modulus, yield stress and break stress compared to synthesised membranes. However, the elongation at break of nonwo-

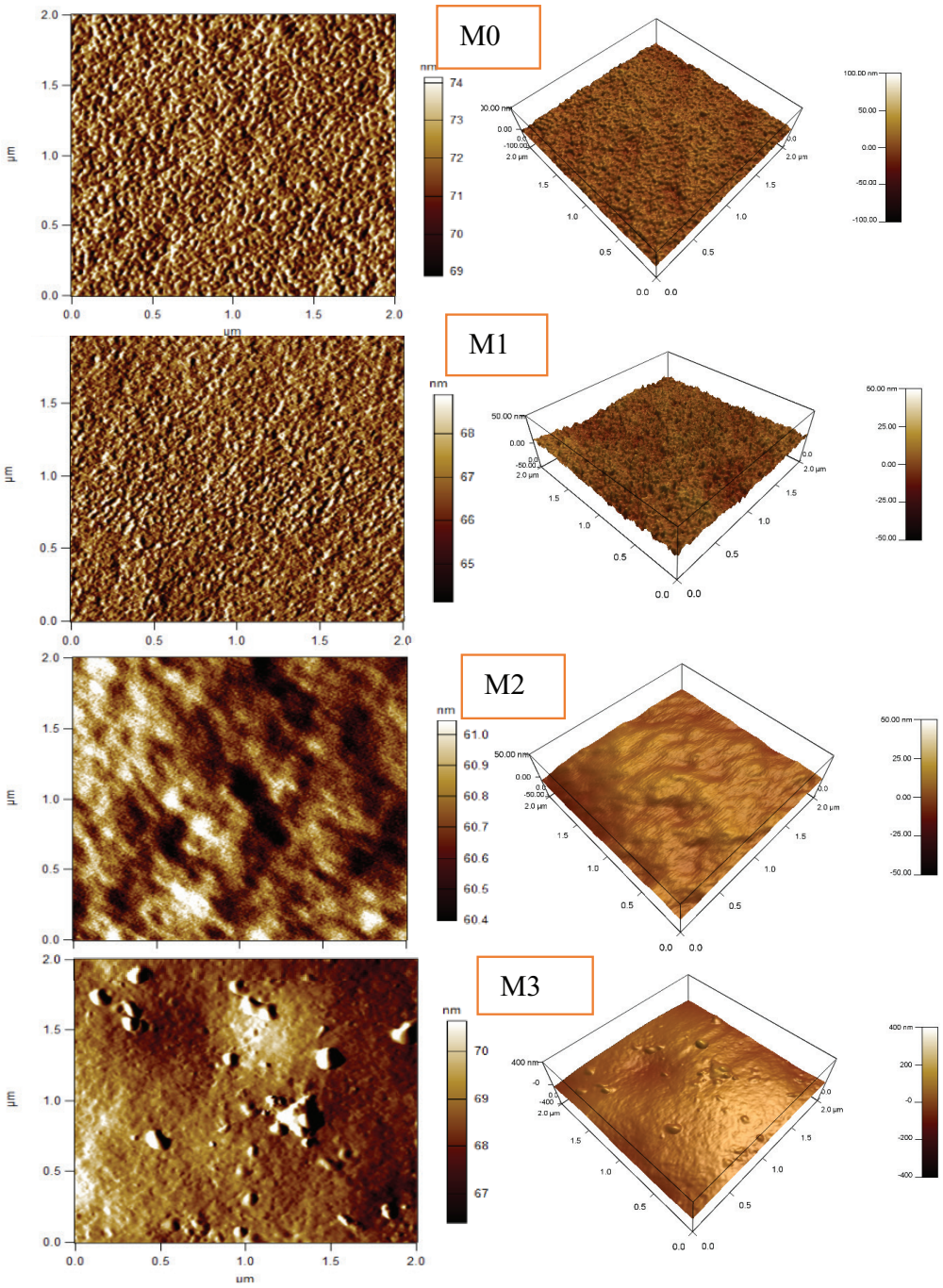

Fig. 10. AFM images of the surfaces and 3D of the PSf and composite membranes.

ven support increased with other casted membranes layer. This is because the nonwoven support was tested under dry conditions and the membranes were studied under wet conditions.

Obtained results show that for M1, the Young's modulus, yield stress and break stress increased and the elongation at break decreased compared to the nonwoven support. The increase in Young's modulus, yield stress and break stress is due to the addition of rigid Filtralite fillers and the decrease of break stress is probably due

Table 3
Porosity, pore size and Roughness data of composite membranes

Membrane	Porosity (%)	Average surface pore diameter (nm)	Roughness RMS (nm)
M0	51.2	5.00 ± 8	6.39
M1	52.1	14.24 ± 6	5.45
M2	56.3	12.82 ± 3	5.12
M3	54.1	8.86 ± 2	5.21

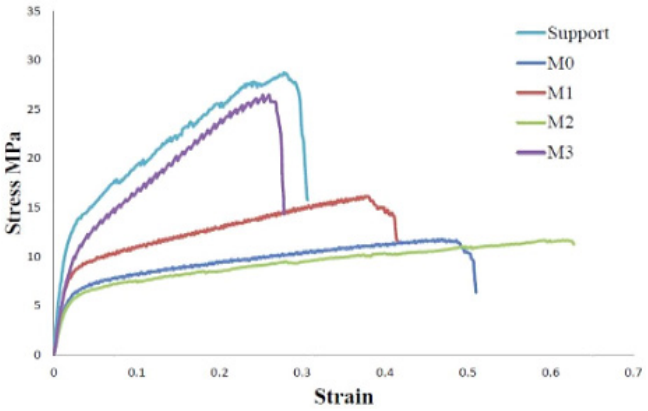

Fig. 11. Mechanical stability of PSf-Filtralite ccomposite membranes.

Fig. 12. Pure water flux of composite membranes.

to the stress concentration around the PSf-Filtralite interface, resulting in de-bonding of the filler/matrix and a decreased break strain. M2 membrane had the lowest mechanical strength among other membranes. High filler content allows for more stress transfer from polymer membranes to fillers. The lower break strain is due to the stress concentration where small cracks initiate at the weak points.

3.3. Membrane permeation study

3.3.1. Pure water filtration

Water filtration experiments showed that PSf-Filtrate composite membranes (M1, M2, M3) have higher fluxes compared to M0 membrane. This can be attributed to increased surface hydrophilicity and the macro-porous structure of the membrane resulting from Filtralite content addition. The functionalization of Filtralite into the PSf membrane led to opening of end gaps of the Filtralite causing higher porosity. The pure water flux of fabricated composite membranes is shown in Fig. 12. The increasing trend in pure water flux was similar to that observed for contact angle and hydrophilicity results. It is well known that enhanced hydrophilicity of the membranes can increase the water permeability by attracting water molecules inside the membrane matrix and facilitating their permeation through the membrane. On other hand, the highest average pore size obtained for M2 membrane which is almost twice of that of M0 correlates sound with the membranes water fluxes. M2 membrane, despite its smaller pore sizes had a higher water flux than M0 due to its higher porosity and improved surface hydrophilicity. However, deposition of clay layer on M3 membrane surface reduced the membrane flux as a result of blockage of membrane pores and/or water channels. Furthermore, the hydrophilicity nature of Filtralite could enhance the solvent and non-solvent exchange during the phase inversion process and lead to membranes with more porous surface, which improved the water permeability. However, for M3, with increased viscosity of the casting solution, reduced the porosity and mean pore radius of the membranes and hence their permeability [43].

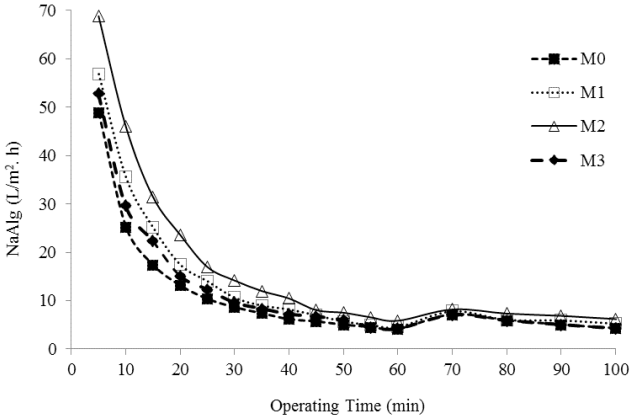

Fig. 13. Flux behavior of membranes during filtration of NaAlg solution.

3.3.2. NaAlg filtration

Filtration experimental results using NaAlg solution are presented in Fig. 13. Results obtained using 0.7 g/L NaAlg solution with a cross flow velocity of 1.7 LPM under a transmembrane pressure (TMP) of 3 bars and temperature of 30°C, show a sharp solution flux decline in all composite membranes. A maximum flux drop in all membranes was observed within the first hour of filtration. Higher NaAlg flux was observed in both M1 and M2 membranes compared to pure PSf membrane (M0) following the same NaAlg rejection trend observed when Filtralite content increased to 1–2% (Table 2). However, an opposite behaviour was encountered for both sodium alginate flux and rejection in M3. This behaviour is attributed to Filtralite agglomeration on M3 membrane surface and incompatibility effect of clay and polymer, resulting in micro phase separation and formation of very few pores on the surface of the membrane [44]. The obtained flux recovery ratio (FRR %) for PSf-Filtralite membranes M1, M2 and M3 was 65.0, 71.0 and 63.0% respectively, while that of M0 was equal to 58% which is in accordance with the literature [45].

3.3.3. Humic acid filtration

Humic acid (HA) filtration tests were carried out 0.75 g/L solution having a cross flow velocity of 1.7 L/min under a transmembrane pressure (TMP) of 3 bars at a temperature of 30°C Using the same cross flow apparatus. Obtained results shown in Fig. 14 present a sharp decrease in HA flux within the first 25 min and continues decreasing until eventually reaching a stable state after 90 min. This decline is caused by HA adsorption on the membrane pores causing the build-up of concentration polarization [46]. HA has a highly active surface characterized by hydrophilic –COOH and –OH functional groups and hydrophobic central aromatic groups and fat molecules [47], hence, HA can be easily deposited on the membrane surface and pores especially that PSf membrane hydrophobicity ensured greater interaction between the membrane surface and Humic acid resulting in strong adsorption and significant flux decline [46,48]. Composite membranes M1 and M2 show better filtration performance due to their improved hydrophilic surface which caused less aggregation of humic acid. Larger flux decline observed in M3 membranes may be attributed to the deposition of large aggregates of Filtralite that induced complete pore blockage or channel constriction, followed by cake formation. Finally, these results showed that hydrophobic PSf membrane was more susceptible to HA fouling than composite membranes. A comparison between the overall flux decline for NaAlg and humic acid showed that the flux decline is higher for NaAlg compared to humic acid solution because of the thinner adsorption layer of NaAlg on the membrane surface compared to humic acid cake layer.

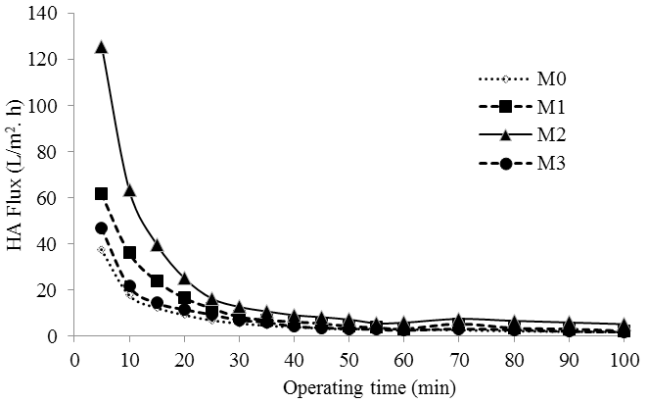

Fig. 14. Flux behavior of membranes during filtration of HA solution.

4. Comparison

A good number of studies have been reported in the open literature on the use clay as membrane filler for filtration applications. The available reported literature data in terms of pure water flux, hydrophilicity and porosity are summarized in Table 5 and compared with data obtained in the present work. Comparison results showed that membranes prepared in our labs in this work performed better than those reported in the literature.

5. Conclusions

New Filtralite-polysulfone composite membranes with enhanced surface morphology and better filtration performance were developed in our laboratory. The addition of Filtralite into the polymer matrices enhanced the mechanical and thermal properties of the membrane. SEM images indicated remarkable changes in the membranes structure and better finger-like channels connectivity. The addition of Filtralite significantly improved the porosity, surface roughness, hydrophilicity and water uptake of the produced membranes. Filtration performance tests results showed improved membrane characteristics in terms of water, HA and NaAlg permeation compared to pristine PSf membrane up to 2% Filtralite addition. However, addition of 3% Filtralite caused a drop in the membrane filtration performance owing to Filtralite particle agglomeration and denser surface morphology. Overall, the addition up to 2% Filtralite concentration improved the overall membranes characteristics beyond which, a reduction in overall parameters was noted.

Acknowledgments

This paper was made possible by an NPRP Grant # 5-1425-2-607 from the Qatar National Research Fund (a member of Qatar Foundation). The statements made herein are solely the responsibility of the authors.

The Authors acknowledge the kind assist of Mr. Moinuddin Yusuf from Center of Advanced Materials (CAM), Qatar University, for providing contact angle and AFM analysis.

Table 4
Detailed mechanical properties of composite membranes

	Fabric (Support)	M0	M1	M2	M3
Thickness (mm)	0.17	0.23	0.24	0.22	0.26
Young's modulus (MPa)	996.56±32.0	494.92±32.8	636.47±11.8	479.66±37.4	599.98±51.8
Maximum tensile stress (MPa)	28.75±0.27	12.10±1.56	16.11±0.16	11.69±0.43	26.43±0.09
Elongation at break %	32.65±1.54	37.70±11.28	38.56±4.54	61.23±1.95	28.07±0.33
Yield stress (MPa)	13.90±0.14	7.43±0.38	9.36±0.18	6.78±0.27	11.27±0.90

Table 5
Summary of available PSf-Filtralite composite membranes

Membrane specifications	Membrane porosity (%)	Hydrophilicity (A°)	Normalized flux PWF (L h^{-1} m^{-2} bar)	Ref
Polymer: PSf	–	Control = 80	Control = 0.29	[43]
Clay Type: Neat MMT		1% Clay = 79	2% neat Clay = 0.54	
2, 3, and 5%		2% Clay = 80	5% neat Clay = 0.25	
		5% Clay = 80	2% MMT-93A = 7.42	
		2% Clay-93A = 79	2% MMT-30B = 96.01	
		2% Clay-30B = 70	5% MMT-30B = 113.36	
		5% Clay-30B = 64		
Polymer: PSf	–	Control = 74.5	Not evaluated	[24]
Clay Type: Neat MMT		0.5% Clay = 72.2		
Clay Dosage: 0.5, 3%		3% Clay = 71.5		
Polymer: PES	–	Control = 57	Control = 1.13	[32]
Clay Type: Neat MMT		2% Clay = 51	4% Clay = 4.67	
Clay Dosage: 0.5 to 10%		4% Clay = 40	10% Clay = 2.22	
		10% Clay = 34		
Polymer: PES	–	Control = 59.5°	Control = 176.4	[31]
Clay Type: Neat MMT		1% Clay-SHMP = 64.3	1% Clay-SHMP = 312.5	
Clay Dosage: 1, 2, 2.5, 3, and 5%		2.5% Clay SHMP = 67.2	2.5% Clay-SHMP =222.7	
		5% Clay SHMP = 68.7	5% Clay-SHMP = 63.3	
		1% Clay = 66.7	1% Clay = 185.0	
		2% Clay = 67.2	2% Clay = 389.3	
		3% Clay = 68.4	3% Clay = 227.1	
		5% Clay =69.8	5% Clay = 102.1	
Polymer: PES	Control = 45.2	Control = 80.6	Control = 342	[49]
Clay Type:	1% Clay = 46.4	1% Clay = 80.4	1% Clay = 348	
Organophilic MMT	2% Clay = 46.8	2% Clay = 80.1	2% Clay = 350	
Clay Dosage:	3% Clay = 46.9	3% Clay = 80.0	3% Clay = 355	
1, 2, 3, 4, 5 and 6%	4% Clay = 47.3	4% Clay = 80.5	4% Clay = 360	
	5% Clay = 47.4	5% Clay = 79.7	5% Clay = 368	
	6% Clay = 48	6% Clay = 80.4	6% Clay = 383	
Polymer-PSf	Control = 34.0	Control = 87.6	Control = 194	[22]
Clay Content: 0 to 6%	1% Clay = 37.1	1% Clay = 86.9	1% Clay = 210	
	2% Clay = 37.4	2% Clay = 86.1	2% Clay = 228	
	3% Clay = 37.7	3% Clay = 84.1	3% Clay = 239	
	4% Clay = 37.9	4% Clay = 83.6	4% Clay = 246	
	6% Clay = 38.6	6% Clay = 82.8	6% Clay = 264	
Polymer: PSf	0% Filtralite = 51.2	0% Filtralite = 70.2	0% Filtralite = 148	Present work
Clay-Filtralite: 0 to 3%	1% Filtralite = 52.1	1% Filtralite = 60.2	1% Filtralite = 378	
	2% Filtralite = 56.3	2% Filtralite = 51.2	2% Filtralite = 447	
	3% Filtralite = 54.1	3% Filtralite = 63.7	3% Filtralite = 250	

References

[1] M.M. Hasani-Sadrabadi, S.H. Emami, R. Ghaffarian, H. Moaddel, Nanocomposite membranes made from sulfonated poly(ether ether ketone) and montmorillonite clay for fuel cell applications, Energy Fuels, 22 (2008) 2539–2542.
[2] F. Bergaya, G. Lagaly, Chapter 1 General Introduction: Clays, Clay Minerals, and Clay Science, in: B.K.G.T. Faïza Bergaya, L. Gerhard (Eds.) Developments in Clay Science, Elsevier, 2006, pp. 1–18.
[3] H. Heinz, Clay minerals for nanocomposites and biotechnology: surface modification, dynamics and responses to stimuli, Clay Minerals, 47 (2012) 205–230.
[4] V. Mittal, Polymer nanocomposites: Layered silicates, surface modifications, and thermal stability, Thermally Stable and Flame Retardant Polymer Nanocomposites, 2011, pp. 3–28.
[5] Y. Li, H. Ishida, Solution intercalation of polystyrene and the comparison with poly(ethyl methacrylate), Polymer, 44 (2003) 6571–6577.

[6] J.U. Calderon, B. Lennox, M.R. Kamal, Thermally stable phosphonium-montmorillonite organoclays, Appl. Clay Sci., 40 (2008) 90–98.
[7] Ö. Ece, A. Alemdar, N. Güngör, S. Hayashi, Influences of nonionic poly (ethylene glycol) polymer PEG on electrokinetic and rheological properties of bentonite suspensions, J. Appl. Polym. Sci., 86 (2002) 341–346.
[8] J. Dau, G. Lagaly, Surface modification of bentonites. II. Modification of montmorillonite with cationic poly (ethylene oxides), Croatica Chem. Acta., 71 (1998) 983–1004.
[9] S. Plimpton, Fast parallel algorithms for short-range molecular dynamics, J. Comput. Phys., 117 (1995) 1–19.
[10] M. Okamoto, S. Morita, H. Taguchi, Y.H. Kim, T. Kotaka, H. Tateyama, Synthesis and structure of smectic clay/poly(methyl methacrylate) and clay/polystyrene nanocomposites via in situ intercalative polymerization, Polymer, 41 (2000) 3887–3890.
[11] X. Tang, S. Alavi, T.J. Herald, Barrier and mechanical properties of starch-clay nanocomposite films, Cereal Chem., 85 (2008) 433–439.
[12] S.H. Othman, Bio-nanocomposite Materials for food packaging applications: types of biopolymer and nano-sized filler, Agric. Agric. Sci. Procedia, 2 (2014) 296–303.
[13] X. Tang, S. Alavi, T.J. Herald, Barrier and mechanical properties of starch-clay nanocomposite films, Cereal Chem. J., 85 (2008) 433–439.
[14] F.Z. Benabid, L. Rong, D. Benachour, M.E. Cagiao, M. Ponçot, F. Zouai, S. Bouhelal, F.J. Baltá Calleja, Nanostructural characterization of poly (vinylidene fluoride)-clay nanocomposites prepared by a one-step reactive extrusion process, J. Polym. Eng., 35 (2015) 181–190.
[15] M. Nasser, S.A. Onaizi, I. Hussein, M. Saad, M. Al-Marri, A. Benamor, Intercalation of ionic liquids into bentonite: Swelling and rheological behaviors, Colloid. Surf. A: Physicochem. Eng. Asp., 507 (2016) 141–151.
[16] S. Pavlidou, C. Papaspyrides, A review on polymer–layered silicate nanocomposites, Progr. Polym. Sci., 33 (2008) 1119–1198.
[17] M. Iman, K.K. Bania, T.K. Maji, Green jute-based cross-linked soy flour nanocomposites reinforced with cellulose whiskers and nanoclay, Ind. Eng. Chem. Res., 52 (2013) 6969–6983.
[18] R.N. Darie, E. Pâslaru, A. Sdrobis, G.M. Pricope, G.E. Hitruc, A. Poiată, A. Baklavaridis, C. Vasile, Effect of nanoclay hydrophilicity on the poly(lactic acid)/clay nanocomposites properties, Ind. Eng. Chem. Res., 53 (2014) 7877–7890.
[19] S.C. George, S. Thomas, Transport phenomena through polymeric systems, Progr. Polym. Sci., 26 (2001) 985–1017.
[20] H.W. Olsen, E.N. Yearsley, K.R. Nelson, Chemico-osmosis versus diffusion-osmosis, Transportation Research Record, 1990.
[21] S.S. Ray, M. Okamoto, Polymer/layered silicate nanocomposites: a review from preparation to processing, Progr. Polym. Sci., 28 (2003) 1539–1641.
[22] Y. Ma, F. Shi, W. Zhao, M. Wu, J. Zhang, J. Ma, C. Gao, Preparation and characterization of PSf/clay nanocomposite membranes with LiCl as a pore forming additive, Desalination, 303 (2012) 39–47.
[23] P. Anadão, L.F. Sato, H. Wiebeck, F.R. Valenzuela-Díaz, Montmorillonite as a component of polysulfone nanocomposite membranes, Appl. Clay Sci., 48 (2010) 127–132.
[24] A. Sanglimsuwan, N. Seeponkai, J. Wootthikanokkhan, Effects of concentration of organically modified nanoclay on properties of sulfonated poly(vinyl alcohol) nanocomposite membranes, Int. J. Electrochem., 2011 (2011) 6.
[25] L. Unnikrishnan, S. Mohanty, S.K. Nayak, N. Singh, Synthesis and characterization of polysulfone/clay nanocomposite membranes for fuel cell application, J. Appl. Polym. Sci., 124 (2012) E309–E318.
[26] G. Defontaine, A. Barichard, S. Letaief, C. Feng, T. Matsuura, C. Detellier, Nanoporous polymer – Clay hybrid membranes for gas separation, J. Colloid Interface Sci., 343 (2010) 622–627.
[27] T. Jose, S.C. George, M.M. G, H.J. Maria, R. Wilson, S. Thomas, Effect of bentonite clay on the mechanical, thermal, and pervaporation performance of the poly(vinyl alcohol) nanocomposite membranes, Ind. Eng. Chem. Res., 53 (2014) 16820–16831.
[28] J.A. Prince, G. Singh, D. Rana, T. Matsuura, V. Anbharasi, T.S. Shanmugasundaram, Preparation and characterization of highly hydrophobic poly(vinylidene fluoride) – Clay nanocomposite nanofiber membranes (PVDF–clay NNMs) for desalination using direct contact membrane distillation, J. Membr. Sci., 397–398 (2012) 80–86.
[29] I. Genné, W. Doyen, W. Adriansens, R. Leysen, Organo-mineral ultrafiltration membranes, Filtr. Separ., 34 (1997) 964–966.
[30] L. Amilia, Synthesis and Characterization of Clay Filled Polysulfone Membran: The Effect of Composition and Calcination of Clay, 2004.
[31] J.C. Mierzwa, V. Arieta, M. Verlage, J. Carvalho, C.D. Vecitis, Effect of clay nanoparticles on the structure and performance of polyethersulfone ultrafiltration membranes, Desalination, 314 (2013) 147–158.
[32] N. Ghaemi, S.S. Madaeni, A. Alizadeh, H. Rajabi, P. Daraei, Preparation, characterization and performance of polyethersulfone/organically modified montmorillonite nanocomposite membranes in removal of pesticides, J. Membr. Sci., 382 (2011) 135–147.
[33] T. Saltnes, B. Eikebrokk, H. Ødegaard, Contact filtration of humic waters: performance of an expanded clay aggregate filter (Filtralite) compared to a dual anthracite/sand filter, Water Sci. Technol.: Water Supply, 2 (2002) 17–23.
[34] I. Masselin, L. Durand-Bourlier, J.-M. Laine, P.-Y. Sizaret, X. Chasseray, D. Lemordant, Membrane characterization using microscopic image analysis, J. Membr. Sci., 186 (2001) 85–96.
[35] S.B. Teli, S. Molina, A. Sotto, E.G. Calvo, J.d. Abajob, Fouling resistant polysulfone–PANI/TiO_2 ultrafiltration nanocomposite membranes, Ind. Eng. Chem. Res., 52 (2013) 9470–9479.
[36] T.L. Barr, S. Seal, H. He, J. Klinowski, X-ray photoelectron spectroscopic studies of kaolinite and montmorillonite, Vacuum, 46 (1995) 1391–1395.
[37] G. Lisa, E. Avram, G. Paduraru, M. Irimia, N. Hurduc, N. Aelenei, Thermal behaviour of polystyrene, polysulfone and their substituted derivatives, Polymer. Degrad. Stability, 82 (2003) 73–79.
[38] S. Karaborni, B. Smit, W. Heidug, J. Urai, E. van Oort, The swelling of clays: molecular simulations of the hydration of montmorillonite, Science, 271 (1996) 1102–1104.
[39] Minerals in Soil Environments, Soil Science Society of America, Madison, WI, 1989.
[40] H. Dong, L. Wu, L. Zhang, H. Chen, C. Gao, Clay nanosheets as charged filler materials for high-performance and fouling-resistant thin film nanocomposite membranes, J. Membr. Sci., 494 (2015) 92–103.
[41] J. Adewole, L. Jensen, U. Al-Mubaiyedh, N. von Solms, I. Hussein, Transport properties of natural gas through polyethylene nanocomposites at high temperature and pressure, 2012.
[42] J.K. Adewole, I.A. Hussein, U.A. Al-Mubaiyedh, Development of a mathematical model for natural gas permeation through polymer nanocomposites at high pressure and temperature, J. Nano Res., 21 (2013) 95–101.
[43] O. Monticelli, A. Bottino, I. Scandale, G. Capannelli, S. Russo, Preparation and properties of polysulfone–clay composite membranes, J. Appl. Polym. Sci., 103 (2007) 3637–3644.
[44] A.K. Ghosh, R.C. Bindal, P.K. Tewari, Preparation of silica-polysulfone based high flux fouling resistant nanocomposite ultrafiltration membranes for separation of proteins, polysaccharides and humic substances, J. Macromol. Sci., Part A, 52 (2015) 299–306.
[45] S. Prabhakar, A.K. Ghosh, R.C. Bindal, P.K. Tewari, Outside skin tubular ultrafiltration membranes for separation of proteins and polysaccharides and removal of turbidity from seawater, Desal. Water Treat., 27 (2011) 231–236.

[46] W. Yuan, A.L. Zydney, Humic acid fouling during ultrafiltration, Environ. Sci. Technol., 34 (2000) 5043–5050.
[47] H.A. Mousa, Investigation of UF membranes fouling by humic acid, Desalination, 217 (2007) 38–51.
[48] M. Pontié, A. Thekkedath, K. Kecili, H. Dach, F. De Nardi, J. Castaing, Clay filter-aid in ultrafiltration (UF) of humic acid solution, Desalination, 292 (2012) 73–86.
[49] Y. Ma, F. Shi, Z. Wang, M. Wu, J. Ma, C. Gao, Preparation and characterization of PSf/clay nanocomposite membranes with PEG 400 as a pore forming additive, Desalination, 286 (2012) 131–137.